Chapter 5

The impact of surface structure and band gap on the optoelectronic properties of Cu_2O nanoclusters of varying size and symmetry

Abstract

A systematic characterization of Cu_2O nanoclusters using classical electrodynamics and time-dependent density functional theory (TDDFT) is performed to investigate their response to light with the alteration of size and symmetry. Absorption and scattering play a crucial role to tune the surface plasmon resonance (SPR), which is the focal feature of optoelectronic properties. In larger dimension the SPR is found to be strongly influenced by scattering and in smaller NPs it is dominated by absorption. A blue shift of the SPR peak is observed with decreasing cluster size. The optical properties of Cu_2O nanoclusters are also affected by the symmetry aspect. With the variation of size and symmetry the associated surface structure and band gap are also varied. The TDDFT calculation is performed to explore the impact of these two fundamental factors on optoelectronic nature of $(Cu_2O)_n$ clusters. The TDDFT study on Cu_2O nanoclusters reveals the nature of electronic excitations in photo irradiated $(Cu_2O)_n$ clusters for n =1, 2, and 3. The transitions involved in $(Cu_2O)_n$ are basically categorized as ligand to metal charge transfer (LMCT) and metal to metal charge transfer (MMCT) processes. The change in absorption with varying cluster dimension and symmetry is found to be critically controlled by the relative probabilities of LMCT and MMCT processes. A competing surface reconstruction effect and occupied-virtual energy gap is also found to govern the SPR pattern of the Cu_2O nanoclusters. All these observations provide an appropriate guideline to tune SPR of Cu_2O NPs for specific applications.

5.1 Introduction

Multifarious application of optoelectronic properties of nanoparticles (NPs) tantalize scientific community to take a closer look at the interior of photo-responsive nanoclusters.[1,2] The central theme of this field of research has been the study of Surface Plasmon Resonance (SPR), which is defined as the collective oscillation of electrons brought about by the irradiation of light.[3-5] The noble metal nanoparticles are the main representatives of SPR till date.[6-8] Interestingly, a number of semiconductor materials have also been found to be SPR-active and can be explored for potential applications.[9-12] Through modification of the size and shape of NPs, the plasmon wavelength can be tuned for a wide range of applications such as in catalysis, optics, chemical and biological sensing, and medical therapeutics.[13-17]

The effect of size of NPs on SPR has already been explored in terms of surface area to volume ratio (*S/V*).[18] Along with the size, alteration in the shape of NPs also changes the *S/V* ratio.[19] With the variation of *S/V*, surface reconstruction takes place.[20-22] The surface reconstruction creates energy levels in the forbidden energy gap of bulk component which is responsible for change in optoelectronic property of semiconductor NPs.[10] Pitarke *et al.* have reported that SPR can be evaluated by dynamical structure factor,[23,24] inverse dielectric function, and screened interaction which vary with shapes.[25] According to Maxwell, dielectric function is the key operator to characterize the optical property of NPs. Except for the sphere, the solution of Maxwell equation for other arbitrary shaped Nps are very limited.[26,27] Noguez has explored the shape effect by spectral representation formalism where polarizability and dielectric function are considered as spectral variables.[2] Coronado *et al.* have suggested the geometrical probability model which exhibits the size and shape dependent contribution to the dielectric function of material in terms of mean free path $(L_{eff}) = 4V/S$.[28]

Though the effect of shape on optical properties is well understood in terms of dielectric function and polarizability, which vary with *S/V* ratio, the connection between the symmetry and optical properties is not yet properly addressed. Lowering of symmetry leads to extension of photonic band gap (PBG) in photonic crystals,[29,30] which undoubtedly infers a pronounced effect

of symmetry on energy gap shift (ΔE). In this work, the role of electronic transitions engaged in collective excitation of electrons is also cultivated. To evaluate the effect of band gap on optoelectronic properties in NPs of different size and shape, Discrete Dipole Approximation (DDA) [31-34] based on electrodynamic method is employed. The absorption, scattering and extinction spectra are computed on NPs with different shapes, such as nanospheres, nanocubes and nanocylinders. Optoelectronic property basically depends on valence electron density. The core electronic part belonging to periodic nature has no significant role to tune this property. The surface atoms of a nanoparticle are not periodic; unlike the bulk core which resemble periodic structure. Insufficient bonding and imperfect coordination number of surface atoms leads to variation in the hybridization of atomic orbitals (AOs). Due to this change in the composition of molecular orbitals (MOs), the nature of electronic excitation becomes distinct, which in turn brings about the diversity of optical response of nanoclusters of different sizes and shapes. Therefore, surface reconstruction has a sound impact in tuning optoelectronic nature of NPs. In this connection, the electronic excitations of small Cu_2O molecular clusters of varying size and symmetry are computed in the platform of Time Dependent Density Functional Theory (TDDFT).[35-38] Each atom in the nano-clusters sits in a different environment from that in the bulk structure, and hence is treated as surface atom in TDDFT calculation. Subsequently larger nanoclusters (of diameter 1 nm and 1.2 nm) are also considered to substantiate the nature of electronic and optical properties of the small clusters, with concomitant verification of the bulk nature of the core part. This deviation of electronic configuration in surface structure with respect to bulk structure enables the proper mapping of DDSCAT data with TDDFT results. Hence, the present work plans to systematically change the size and symmetry of the NPs so as to examine the correlated variation in surface structure reconstruction and band gap, which partakes in tuning the optoelectronic properties of NPs.

As a representative congener of this study, we choose Cu_2O nanoparticle for its interesting exitonic features.[39-45] Cuprous oxide (Cu_2O) is a *p*-type semiconductor with a band gap of 2.2 eV.[46] Due to its high optical absorption coefficient, it is potentially used for gas sensing,[47] solar energy photovoltaics,[48-51] photocatalysis,[52-54] cell imaging and for identification of proteins.[55] Various interesting Cu_2O nanostructures such as nanocubes,[56-59] octahedra,[46,60-62] nanospheres,[63-65] nanocages,[66-68] hollow spheres,[69] nanowires,[58,70] nanorods and other highly

symmetrical structures have been reported.[71,72] Cu_2O NPs not only lead to the local structural alteration of proteins but also acts as a novel optical probe applied in cell or molecular biology imaging.[73] The effect of band gap variation and surface reconstruction on the optoelectronic properties of Cu_2O NPs are understood by altering the size of NPs with different shape symmetries, namely sphere, cube and cylinder, through Discrete Dipole Approximation. In order to draw a meaningful quantum chemical interpretation of the DDA simulation results, the electronic excitations in the optimised structures of $(Cu_2O)_1$, $(Cu_2O)_2$ and $(Cu_2O)_3$ are performed in the platform of time-dependent density functional theory (TDDFT). The effect of variation in size is investigated keeping the symmetry constant at C_{2v}. On the other hand, the variation in symmetry from C_s to C_{3v} is studied keeping the size constant at $(Cu_2O)_3$. For convenience, electronic excitations in larger and more realistic cluster of 1 nm diameter ($[Cu_{28}O_{15}]^{6+}$) and 1.2 nm diametr ($[Cu_{44}O_{15}]^{6+}$) are also computed. The comprehensive comparison of optical properties of Cu_2O nanoclusters having different size and symmetry guides the proper selection of nanoparticles for specific bio-medical applications and therapeutic uses.

5.2 Theoretical Background and Computational Details

5.2.1 DDA Simulation Method

The computation of optical response of isolated NPs of different shapes and sizes are performed using the Discrete Dipole Approximation algorithm implemented in the DDSCAT 7.1.0 code developed by Draine and Flatau.[31] The isolated nanoparticles are represented as a lattice of polarizable cubic elements (N-point dipoles) with positions and polarisabilities r_i and $\alpha_i (i = 1,2,.....,N)$ respectively. The target is excited by monochromatic incident plane wave. The polarization induced in each dipole is expressed as

$$P_i = \alpha_i \bullet E_{loc,i}(r_i). \tag{5.1}$$

Here $E_{loc,i}(r_i)$ is the local field, which is the sum of the incident radiation field and the field radiated by the other N 1 dipoles. For a given value of incident wavelength λ, the field can be expressed as

$$E_{loc,i}(r_i) = E_{inc,i} + E_{dip,i} = E_0 \exp(ik \cdot r_i) - \sum_{j \neq i} A_{ij} \cdot P_j \tag{5.2}$$

Where E_0 and $k = \frac{2\pi}{\lambda}$ are the amplitude and wave number of the incident wave respectively. The interaction matrix A can be represented as

$$A_{ij} \cdot P_i = \frac{\exp(ik|r_{ij}|)}{|r_{ij}|^3} \left\{ k^2 r_{ij} \times \left(r_{ij} \times P_j \right) + \frac{\left(1 - ik|r_{ij}|\right)}{|r_{ij}|^2} \times \left[|r_{ij}|^2 P_i - 3 r_{ij} \left(r_{ij} \cdot P_j \right) \right] \right\} \tag{5.3}$$

$j = 1, 2, ..., N, \qquad j \neq i$

Where $|r_{ij}| = |r_i - r_j|$ and P is the polarization vector. Substituting eq 5.2 and 5.3 into eq 5.1 and with subsequent rearrangement one gets

$$A' \cdot P = E \tag{5.4}$$

The matrix A' is derived from the matrix A of equation 3 and is a $3N \times 3N$ matrix for a target with a total of N dipoles. E and P in equation 5.4 are $3N$ dimensional vectors. The polarization vector P can be obtained by solving these $3N$ linear equations. Then the extinction and absorption cross sections of the NPs can be calculated by

$$C_{ext} = \frac{4\pi k}{|E_0|^2} \sum_{i=1}^{N} \mathrm{Im}\left(E^*_{loc,i} \ . \ P_i \right) \tag{5.5}$$

$$C_{abs} = \frac{4\pi k}{|E_0|^2} \sum_{i=1}^{N} \left\{ \mathrm{Im}\left[P_i \ . \ \left(\alpha_i^{-1} \right)^* P_i^* \right] - \frac{2k^3}{3} |P_i|^2 \right\} \tag{5.6}$$

Here $*$ implies complex conjugate.[74] The scattering cross section is obtained from the following relati

$$C_{ext} = C_{sca} + C_{abs}. \tag{5.7}$$

The extinction efficiency (Q_{ext}), absorption efficiency (Q_{abs}), and scattering efficiency (Q_{sca}) are obtained through the following set of equations

$$Q_{ext} = \frac{C_{ext}}{\pi\ a_{eff}^2}$$

$$Q_{abs} = \frac{C_{abs}}{\pi\ a_{eff}^2} \tag{5.8}$$

$$Q_{sca} = \frac{C_{sca}}{\pi\ a_{eff}^2}$$

Where a_{eff} is the effective radius of a sphere with volume ($\frac{4\pi a_{eff}^3}{3}$) equal to the volume of the particle of any arbitrary shaped NP.

5.2.2 TDDFT Method

For the calculation of excitation energy of molecular clusters the unrestricted density functional formalism is adopted, which is implemented in the Amsterdam Density Functional (ADF) program.[75,76] The ground states of all molecular clusters are studied within the Local Density Approximation (LDA)[77] and Generalized Gradient Approximation (GGA).[78] For the GGA, the Becke's exchange[79] and Lee-Yang-Parr correlation[80] functional (BLYP) is chosen. The double-ζ (DZ) and the triple-ζ with double polarization (TZ2P) Slater type basis sets are

used for geometry optimization. To check the vibrational stability of the clusters, all the frequencies and normal modes are calculated using both of the prior mentioned approximations (LDA and GGA). To calculate the excitation energy within frozen core condition, LB94[81] is employed as exchange and B3LYP[82] as correlation functional. The basis sets employed is similar to that used in geometry optimization process.

5.3. Results and Discussion

5.3.1 DDA calculation

The calculations are performed for spherical, cubic and rod shaped Cu_2O nanoparticles. In order to produce accurate result from DDA, the inter-dipole separation *d* should be made smaller than the structural length of the target.[83] Hence, with the decrease in the target size; the dipole size is also reduced. Thus the typical cube size of each dipole is altered from 3.0 nm to 1.5 nm with subsequent variation in the number of dipoles (*N*) from 2.6×10^5 to 4.5×10^3. Though, polarizability α_i depends on the refractive index of Cu_2O; [84] here the nanoparticles are assumed to be embedded in vacuum with refractive index one. The incident wavelength is varied from 150 nm to 750 nm.

5.3.2 Effect of size on absorption and scattering properties

5.3.2.1 Cu_2O Nanospheres

The spherical Cu_2O NPs are found to absorb in the UV region up to a limit of 80 nm in diameter, beyond which the absorption starts to occur at visible spectrum. Hence, the efficiency of absorption (Q_{abs}), scattering (Q_{sca}) and extinction (Q_{ext}) are calculated for Cu_2O nanospheres ranging from diameter (*D*) 100 nm to 240 nm [Figure 5.1(a), (b) and (c)].

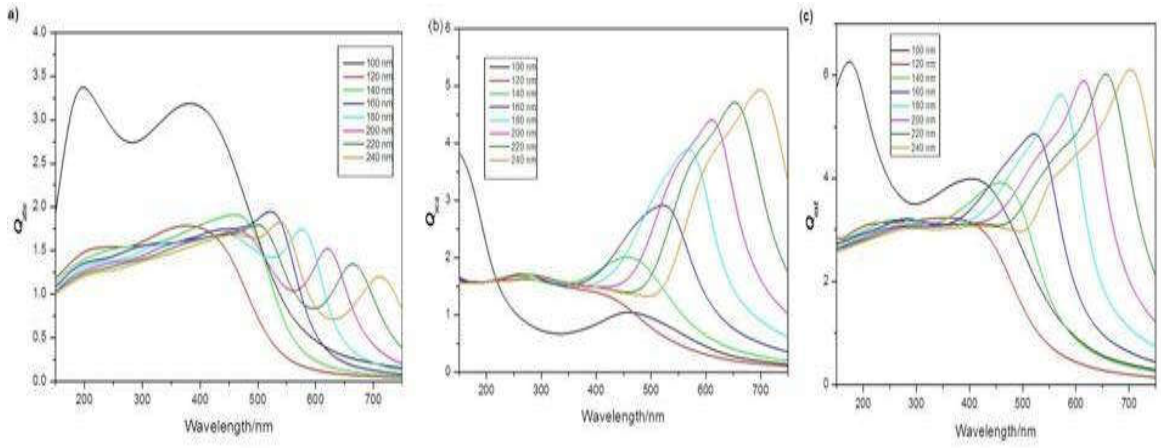

Figure 5.1 Simulated spectra of (a) absorption (b) scattering and (c) extinction of Cu_2O nanospheres with diameter 100 nm to 240 nm

The absorbance is displayed within the wave length region 150 nm to 750 nm. It is evident from the plots that decrease of the particle size causes blue shift of the peaks. A close inspection of the plots also reveals that with decrease in particle dimension there occurs a decrease in scattering and vis-à-vis increase in absorbance of the nanoparticles. As a consequence, the SPR peaks resemble to absorption and scattering peaks in smaller and larger dimensions respectively. This observation suits the relation displayed in equations 5.7 and 5.8. The absorbance of the nanosphere of diameter 220 nm, obtained through DDA simulation is in well agreement with experimental value.[85] This reinforces the accuracy of the DDA simulation, as is reported earlier.[86] The molar absorption (ε_{abs}) and scattering (ε_{sca}) coefficients of nanospheres show a similar variation with size as that of equivalent cross sectional areas, which is in agreement with the proportionality between equivalent sectional area and the coefficients, ε_{abs} and ε_{sca}.[87] The values of ε_{abs} and ε_{sca} in nanospheres, both measured at the same wavelength where SPR shows maximum efficiency, are reported in Table 5.1.

Table 5.1 Calculated molar absorption coefficients (ε_{abs}), molar scattering coefficient(ε_{sca}),Surface area to volume ratio (*S/V*) and band gaps of NPs of varying shapes (sphere, cylinder, cube) and sizes at their corresponding surface plasmon resonance wavelength maximum (λ_{max})

shape		**Size nm**		λ_{max} **nm**	$\varepsilon_{abs} \times 10^{10}$ **$M^{-1}cm^{-1}$**	$\varepsilon_{sca} \times 10^{10}$ **$M^{-1}cm^{-1}$**	**Band gap eV**	***S/V*** **(nm^{-1})**
sphere		Diameter						
		100		404.7	6.46	1.75	2.32	0.06
		120		386.87	5.31	4.36	2.48	0.05
		140		459.79	4.37	8.1	2.29	0.043
		160		522.83	10.2	15	2.17	0.037
		180		576.56	11.6	26	2.03	0.033
		200		622.03	12.5	36	1.7	0.03
		220		663.32	13.4	47	1.65	0.027
		240		711.46	14.4	58	1.64	0.025
cylinder	Long axis	Diameter	Aspect ratio					
	553	34	16.26	181	9.49	5.50	3.24	0.116
	692	40	17.3	197	11.91	6.02	3.18	0.099
	796	54	14.74	229	13.97	6.03	2.89	0.073
	899	57	15.77	249	18.78	7.03	2.81	0.069
	937	63	14.87	233	25.29	9.87	2.89	0.063
	980	72	13.61	403	29.19	10.93	2.52	0.055
	1145	77	14.87	427	38.88	13.26	2.49	0.052
	1385	80	17.31	443	47.39	16.21	2.44	0.050
cube		Diameter						
		100		339.47	4.27	3.2	2.69	0.074
		120		393.09	5.86	4.54	2.46	0.062
		140		454.17	8.31	8.96	2.34	0.053
		160		511.35	10.8	16.7	2.19	0.046
		180		559.24	12.2	28.4	2.04	0.041
		200		603.08	12.9	39.9	1.93	0.041
		220		642.58	13.5	51.2	1.78	0.034
		240		687.98	14.3	63.2	1.65	0.031

The SPR maxima of nanospheres of diameters with 140 nm to 180 nm are close to the reported values (Table 5.1).[88-90] With increase of size, the magnitude of visible light scattering (ε_{sca}) exhibits a steeper increase than ε_{abs}, which is attributed to the decrease of band gaps with increasing size of NPs. (Table 5.1, Figure 5.2).

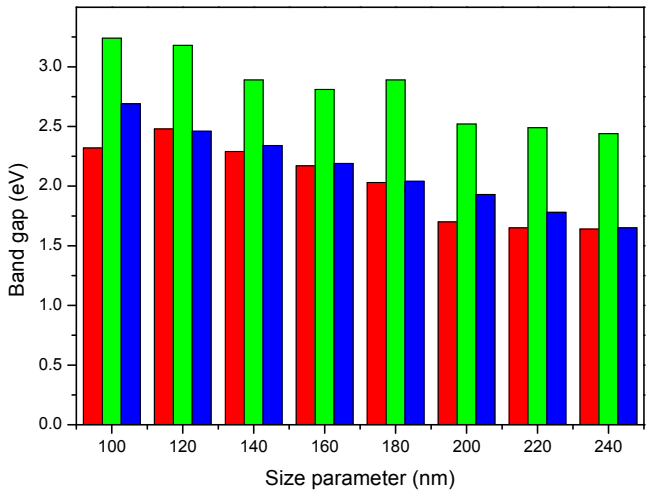

Figure 5.2 Variation of calculated band gaps of spheres (red), cylinders (green) and cubes (blue) with increasing size parameters

This observation is in qualitative agreement with the experimental findings for other semiconductors also.[91] Here, the band gap (E_g) is estimated from the absorbance spectra,

$$\varepsilon_{abs} \approx A(h\nu - E_g)^n \qquad (5.9)$$

Where, A is a frequency independent constant, $h\nu$ is the energy of photons, n in the index depends upon the type of transition. For direct allowed band gap $n = \frac{1}{2}$.[92] The calculated band gaps are close to the value of bulk band gap and the trend of variation of the band gap values also

follow the literature.[93] The spectra for efficiency of absorption shows two distinct peaks at larger dimension of the NPs. With the decrease in size, these two peaks approach each other and ultimately merge to a hump at a diameter of 120 nm (Figure 5.1 a).

5.3.2.2 Cu_2O Nanocylinders

The variation of Q_{abs} , Q_{sca} and Q_{ext} in Cu_2O nanocylinders with the change in the aspect ratio (height/diameter or long-axis/short-axis) is displayed in Figure 5.3

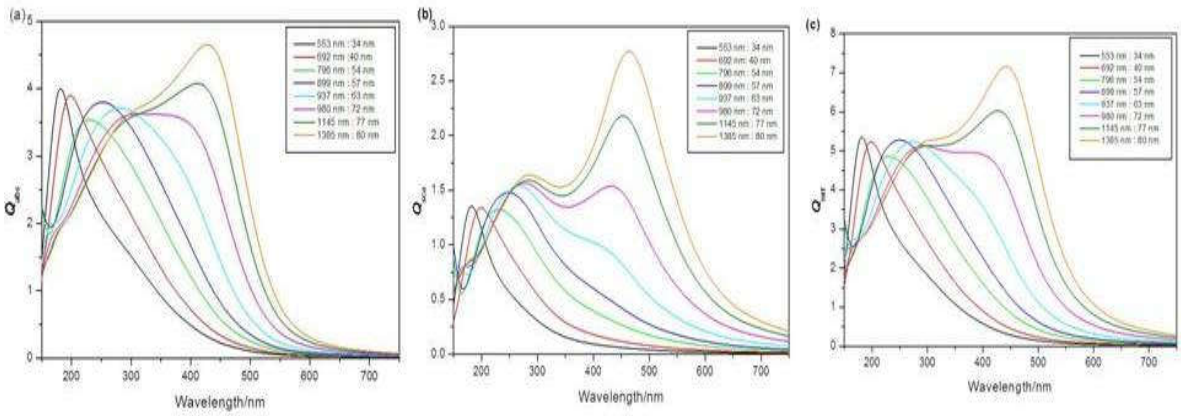

Figure 5.3 Simulated spectra of (a) absorption (b) scattering (c) extinction of Cu_2O nanocylinders with size parameters long axis : diameter from 553 nm : 30 nm to 1185 nm : 80 nm

The aspect ratio of cylinders is varied from 13.6 to 17.3. The aspect ratios of nanocylinders are chosen, so as to be similar to the limiting size range of nanospheres. The resonance along the long axis is known as longitudinal mode which propagates along the direction of the applied field. The mode perpendicular to the applied field is known as transverse mode. Here only the longitudinal mode is considered as it shifts to the visible range of light. Similar to nanospheres, here also the SPR band shifts to the shorter wavelength with decrease of the size parameter (height and diameter) and the ε_{abs} value shows a monotonic decrease as well. Most of the peaks appear in the UV region (<350 nm). This is attributed to the higher band gap in cylinders than spheres. At the lowest value of aspect ratio (13.6) the sharp peaks corresponding to referred modes (transverse and longitudinal) merge to form a hump like curve.

On the contrary, with increase of aspect ratio, the sharpness of the curves increases and the curves corresponding to longitudinal and transverse modes appear as two distinct peaks. However, most of the absorbance appears in the UV region up to 63 nm diameter of nanocylinders. On the other hand, the nanospheres of similar size absorb at around 576 nm. In nanocylinders, the Q_{abs} is higher and Q_{sca} is lower than that in` sphere (Figure 5.4 and Figure 5.5). Compared to sphere, the difference in absorption is attributed to the larger surface area[94] of cylinder which causes increment in the band gap and consequently results in higher absorption intensity (Figure 5.2).

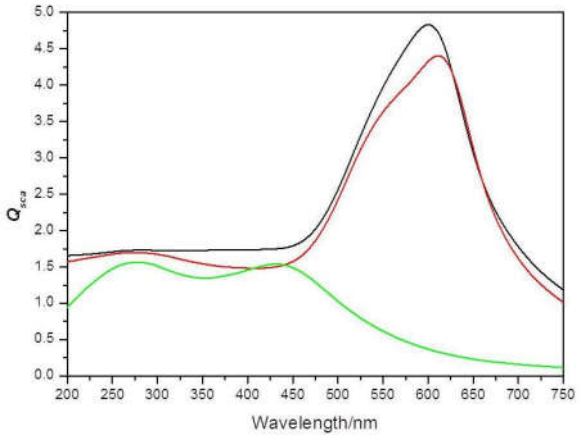

Figure 5.4 Variation of absorption with shapes [sphere (red), cylinder (green), cube (black)] of NPs having equal volume of a sphere with effective radius 100 nm.

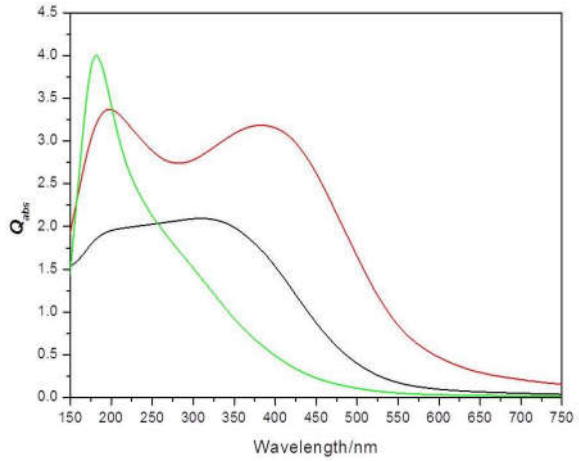

Figure 5.5 Variation of scattering with shapes [sphere (red), cylinder (green), cube (black)] of NPs having equal volume of sphere with effective radius 100 nm.

5.3.2.3 Cu_2O Nanocubes

Similar to Cu_2O nanospheres, the limiting size range of Cu_2O nanocubes for optical response to appear in visible region is 100 nm to 240 nm. The nature of variation of Q_{abs}, Q_{sca} and Q_{ext} parameters with wavelengths for Cu_2O nanocubes are comparable to nanospheres [Figure 5.6 (a), (b) and (c)]. The SPR peaks are blue shifted with decrease in size, similar to the trend in Cu_2O nanospheres and nanocylinders. The calculated ε_{abs} and ε_{sca} values for nanocubes are close to the values of corresponding nanospheres due to comparable band gap values (Figure 5.2). The nanocubes acquire highest scattering coefficient values (ε_{sca}) among three shapes having equal volumes (Table 5.1). The highest efficiency of scattering (Q_{sca}) in nanocubes supports the above observation (Figure 5.5). The calculated band gaps are in the range of 2.69 eV to 1.65 eV (Table 5.1). The nature of spectra of Q_{abs} is analogous to the mentioned shapes with two different peaks which come closure with decrease of size and merge at the size of 100 nm.

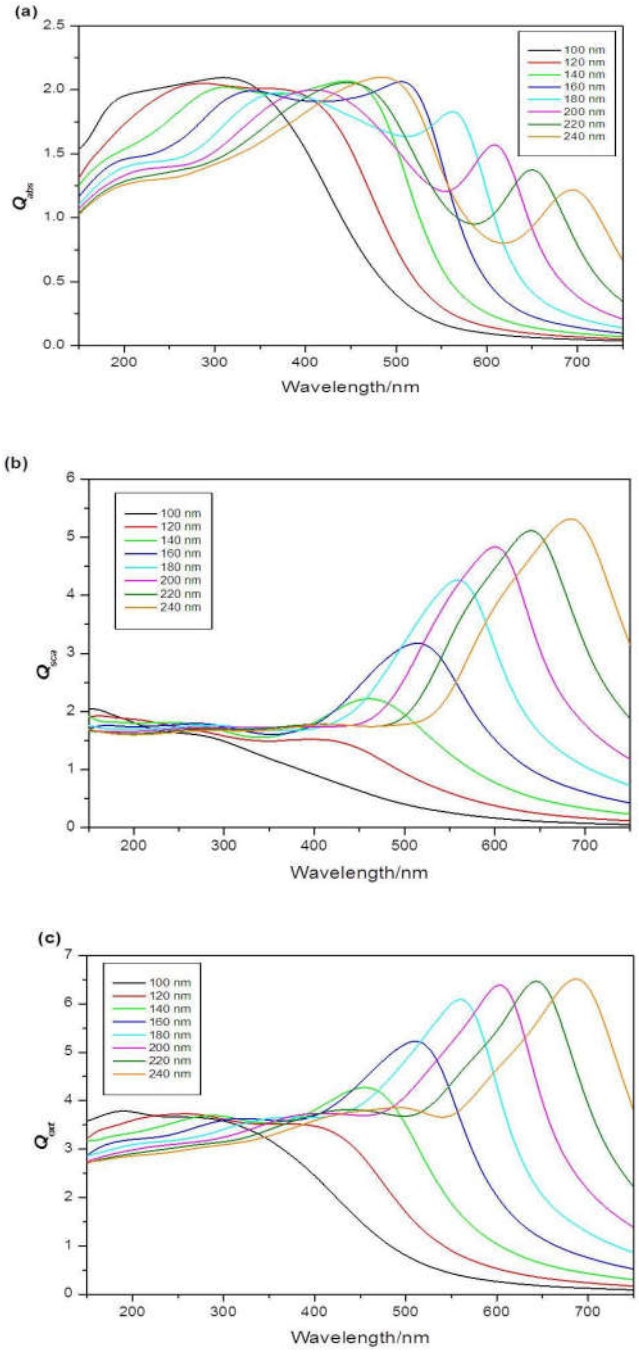

Figure 5.6 Simulated spectra of (a) absorption (b) scattering (c) extinction of Cu_2O nanocubes having equal volume of nanospheres of diameter 100 nm to 240 nm.

5.3.3 Effect of symmetry on absorption and scattering properties

Usually the 3D shapes are represented by several descriptors, of which symmetry and surface area to volume ratio are maximally used. Symmetry is known as shape similarity descriptor and measures the similarity between two 3D shapes. Whereas, surface area to volume ratio (*S/V*) is termed as shape dissimilarity descriptor and measures the dissimilarity between two 3D shapes.[95-99] Though, the dependence of absorption and scattering properties of the nano particle on the *S/V* ratio is well-cultivated;[2, 28, 90-103] the same dependence on the symmetry needs a detail attention. According to nanothermodynamics,[104] with increase of surface area the surface energy increases due to increment of density of elastic strain energy of lattice relaxation, density of dangling bonds and coordination imperfection. This enhancement of surface energy leads to the blue shift of band gap.[105]According to chemical bond theory [106, 107] the optical gap shift (measured from the shift of absorption threshold of nanocrystal with respect to the bulk) appears from two types of effects. First is the quantum effect, responsible for quantum effect shift (ΔE^{kubo}), which arises from the discretization of the band structure due to decrease in the dimension. Second is the surface effect, arising from termination of lattice periodicity on the surface of nanoclusters and responsible for surface effect shift ($\Delta E^{surface}$). Thus, the energy gap shift (ΔE) can be represented as the sum of the two mentioned shifts ($\Delta E = \Delta E^{kubo} + \Delta E^{surface}$).The electronic structure, that defines the optical properties of NP is intimately related to the atomic structure and its symmetry. NPs with higher symmetry exhibit highly degenerate states. Reducing the symmetry split the degenerate MOs leads multiple energy states. Therefore tuning of symmetry affects the energy gap shift (ΔE) in nanoclusters. [108] Since the *S/V* ratio of nanosphere and nanocube is comparable (Table 5.1), the distinction of absorption and scattering properties in those shapes is hardly correlated with surface effect shift ($\Delta E^{surface}$) and symmetry becomes the chief reason behind the difference of their optical properties. To investigate this issue, the absorption and scattering efficiencies of Cu_2O cluster of different symmetries are calculated keeping their size constant (D = 100 nm). The variation of scattering efficiency (Q_{sca}) against different symmetries are shown in Figure 5.5, which delineates highest efficiency for lowest symmetric cube. Hence, aligning with this order, minimum scattering efficiency should be displayed by most symmetric nanospheres. However, opposed to this trend,

the cylinder shape is found to be associated with lowest Q_{sca} and highest value of Q_{abs}. This anomaly can be explained by the highest *S/V* ratio of cylinder compared to other shapes (Table 5.1). A considerable contribution from surface effect ($\Delta E^{surface}$) also acts to enhance the value of ΔE in nanocylinder, for which the band gap becomes highest in case of nanocylinders. In a nutshell, the symmetry turns into an effective parameter to tune the band gap, which is in turn responsible for differentiation of optical response in nanoclusters.

5.3.4 TDDFT calculation

GGA functionals are reported to produce reasonably well prediction of excitation behavior in transition metal complexes.[109] This functional is also found to reproduce the experimentally reported structure as evident from Table S1. Hence, we finalized the optimized structure of the GGA functional for further calculation. A complete list of harmonic frequencies is given in the basic data for the optimized structures considered in this work. $(Cu_2O_3)_3$ cluster with different symmetries imaginary frequencies of magnitude less than 31 cm^{-1} are found. This is reported to be likely due to small inaccuracy in the numerical grid.[110]

5.3.4.1 Effect of size

The TDDFT is exercised to obtain the excitation energy of $(Cu_2O)_1$, $(Cu_2O)_2$ and $(Cu_2O)_3$ clusters in their C_{2v} symmetry (Figure 5.7).

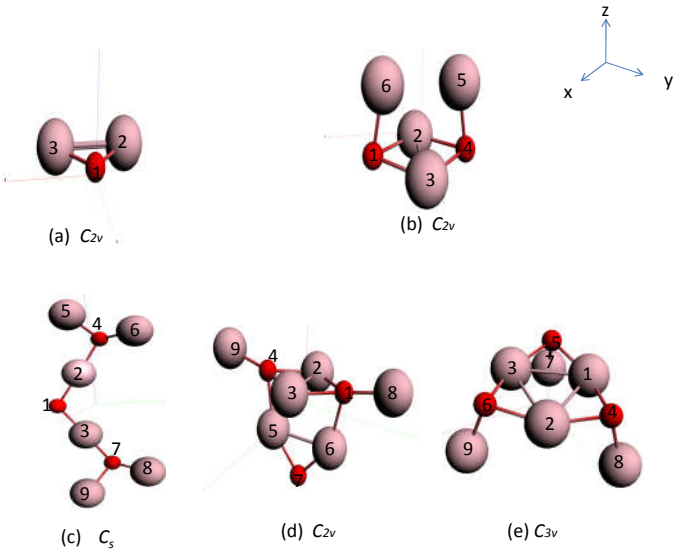

Figure 5.7 Molecular clusters of Cu_2O (a) $(Cu_2O)_1$, (b) $(Cu_2O)_2$, (d) $(Cu_2O)_3$ in C_{2v} symmetry , (c) and (e) are $(Cu_2O)_3$ in C_s and C_{3v} symmetry respectively.

The structural parameters in the optimized geometries of $(Cu_2O)_n$ clusters [n =1, 2, and 3] are found to be in well agreement with the reported bond distance[111,112] (Table S5.3). Analysis of the structure of Cu_2O molecular clusters reveals four different coordination environments for Cu and O atoms which are designated as Cu_{CSA}, Cu_{CUS}, O_{CSA}, O_{CUS}. Here, the CSA and CUS in the suffix imply coordinatively saturated and coordinatively unsaturated respectively following the notations of Soon *et al*.[113] In bulk state, each O atom is surrounded by four tetrahedron Cu atoms and referred to as O_{CSA}. On the other hand, the coordination number varies from two to three in O_{CUS}, which are denoted by O_{CUS}^2 and O_{CUS}^3 respectively. Similarly, Cu_{CSA} and Cu_{CUS} denote copper with coordination number two and one respectively. The alteration in size of the cluster brings about the change in the coordination number of surface atoms, which in turn leads to the change in structural parameters in the clusters.[114-116] Due to the change in coordination with increase of size (in C_{2v} symmetry), the Cu_{CSA} O_{CUS} and Cu_{CUS} O_{CUS} bond lengths decrease and Cu_{CSA} Cu_{CSA} bond lengths increase (Table S5.3). As a consequence, the bond angle $\angle Cu_{CSA}$ O_{CUS} Cu_{CSA} linearly increases with size. The increase in the size of cluster increases the population of surface atoms. Due to unsaturated coordination number, the surface atoms show a greater tendency to participate in the electronic transition for having more valence

electrons compared to the bulk atoms. Thus, the variation in electronic transitions taking place between occupied and virtual MOs in clusters of increasing size is attributed to the reduction in coordination number (Table 5.2). For simplicity, only the peaks with highest oscillator strength (OS) (designated as ***1*** in Figure 5.8) are reported for each cluster.

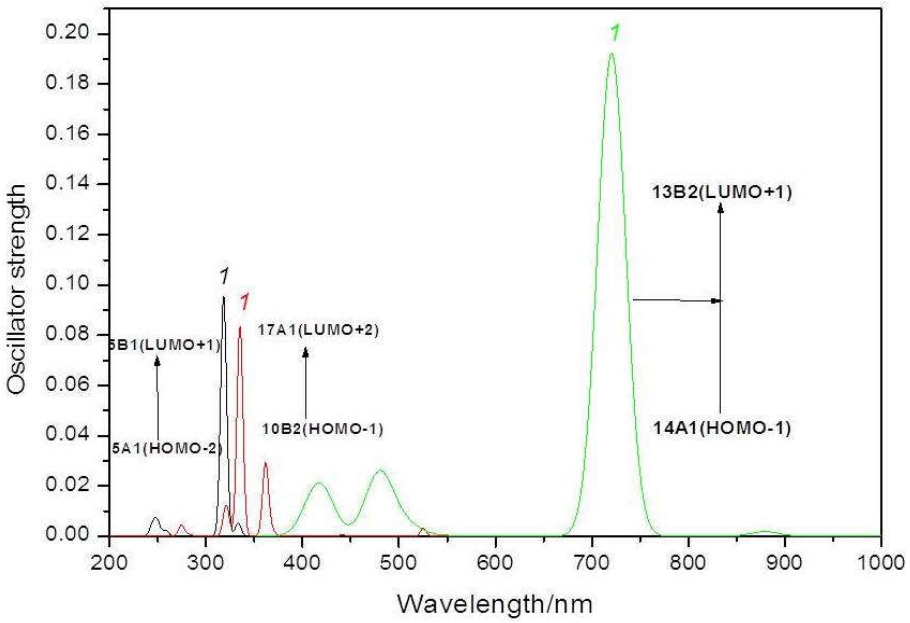

(a)

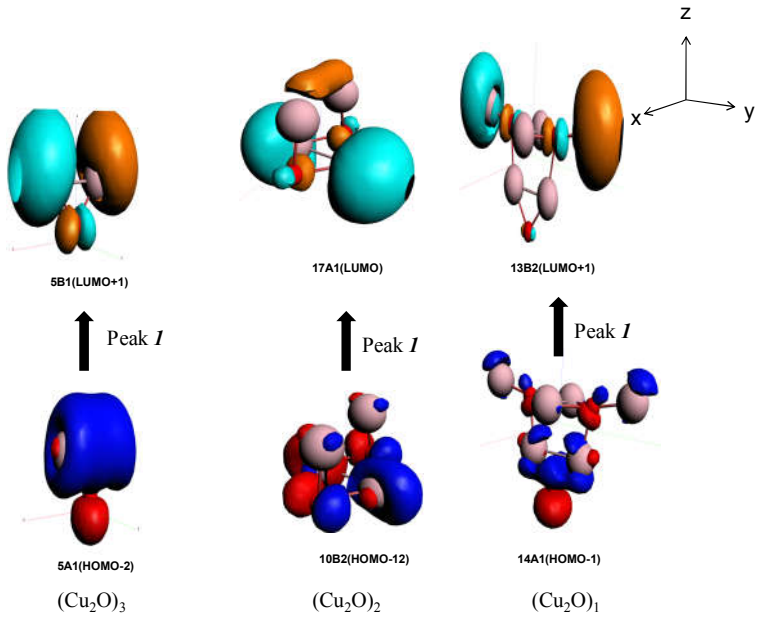

(b)

Figure 5.8 (a) TDDFT valence excitation spectra (oscillator strength vs excitation energy) of$(Cu_2O)_1$ (black), $(Cu_2O)_2$ (red) and $(Cu_2O)_3$ (green) clusters having same symmetry (C_{2v}). Only the most intense discrete transitions are reported and labelled as ***1***. **(b).** The representation of MOs participating in the electronic transitions to form the most intense peaks labelled as ***1*** in $(Cu_2O)_n$ clusters (n = 1, 2 and 3). x, y and z are the reference axis of the MOs

The excitation peaks are directly dependent on the energy gap between occupied and virtual MOs ($\Delta E_{\text{occ-vir}}$), which can be found from Figure 5.8 and Table 5.2. To find out the MO and its component AOs participating in the electronic transition, the partial density of states (PDOS) of fragments is analysed in Table S5.1 of ES5.I. From Table S5.1, it is seen that the occupied MOs are dominated by *p* AOs of O fragments with minor contribution of *d* AOs of Cu fragments. On the other hand the virtual MOs are dominated by *s* and *p* AOs of Cu fragments. Again, $(Cu_2O)_3$ and $(Cu_2O)_2$ are found to have highest and lowest percentage contribution of oxygen *p* AO in their occupied MOs (Figure 5.9a).

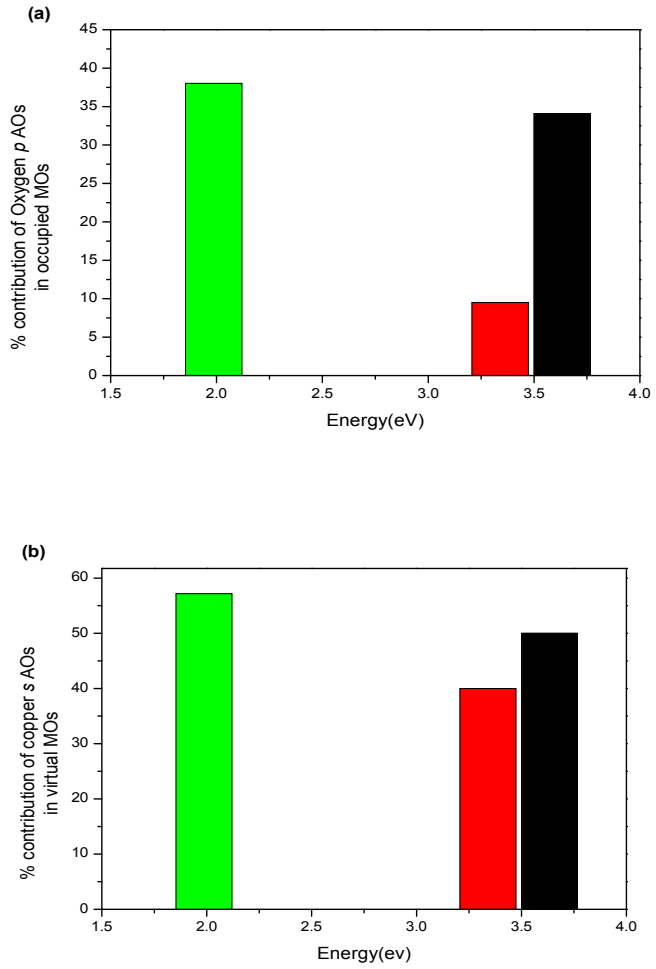

Figure 5.9 Variation of extent of LMCT in terms of % contribution of (a) ligand AOs in occupied MOs and (b) metal AOs in virtual MOs in molecular clusters of $(Cu_2O)_1$(black), $(Cu_2O)_2$ (red) and $(Cu_2O)_3$ (green)

Nevertheless, the OS of electronic transition also increases with increase in percentage contribution of *s* AOs of Cu fragments in virtual MOs [Table 2 and Figure 9(b)].

Table 5.2 Discrete electronic excitations of Cu_2O clusters of different sizes in C_{2v} symmetry calculated through TDDFT and compared with reported values in reference (85)

Clusters	**Symmetry**	**Peaks**	**Occupied orbital**	**Virtual Orbital**	**$\Delta E_{occ-vir}$ (eV)**	**Oscillator strength**	**Excitation Energy (eV)**	**Reported excitation energy[a] (eV)**
$(Cu_2O)_1$	C_{2v}	1	5A1(HOMO-2)	5B1(LUMO+1)	3.42	0.095	3.90	3.54(6.7 nm)
$(Cu_2O)_2$	C_{2v}	1	10B2(HOMO-1)	17A1(LUMO+2)	3.395	0.0822	3.69	2.76(8 nm)
$(Cu_2O)_3$	C_{2v}	1	14A1(HOMO-1)	13B2(LUMO+1)	1.313	0.1923	1.72	2.63(14 nm)

A marked effect of variation of coordination number on the nature of electronic excitation has been revealed from MO diagram analysis (Fig. 5.8). In $(Cu_2O)_1$ and $(Cu_2O)_3$ the peaks designated as ***1*** are basically produced from 5A1 to 5B1 and 14A1 to 13B2 transitions respectively (Table 5.2). Here, nA1, nA2, nB1 and nB2 represent the n-th SCF molecular orbitals as generated in ADF. A1, A2,… are the subspecies of irreducible representation internally used by ADF. The labels A, B and subscripts 1, 2 are associated with standard notations in literature.[117] The source MOs (5A1 and 14A1) are dominated by p_z AOs of $O_{1CUS}{}^2$ and $O_{7CUS}{}^2$ in $(Cu_2O)_1$ and $(Cu_2O)_3$ respectively (The number in the subscript such as 1 and 7 implies the atom number of the clusters depicted in Fig. 5.7). On the other hand, the destination MOs (5B1 and 13B2) are formed through major contributions from *s* AOs of Cu_{2CUS}, Cu_{3CUS} in $(Cu_2O)_1$ and *s* AOs of Cu_{8CUS}, and Cu_{9CUS} in $(Cu_2O)_3$ (Fig. 5.8b). No $O_{CUS}{}^2$ atom is present in $(Cu_2O)_2$. The peak ***1*** in case of $(Cu_2O)_2$ is associated with transition from 10B2 to 17A1 MO. The 10B2 MO is composed of Cu_{2CUS}, Cu_{3CUS} $d_{x^2-y^2}$ AOs and 17A1 MO is composed Cu_{2CUS}, Cu_{3CUS} *s* AOs. Hence from the above discussion it becomes apparent that the nature of

electronic excitation is typically ligand to metal charge transfer (LMCT) in $(Cu_2O)_1$ and $(Cu_2O)_3$ and metal to metal charge transfer (MMCT) in $(Cu_2O)_2$. This observation is in concordance with XPS (X-ray Photoelectron Spectroscopy) study and other quantum chemical computations which concludes that charge transfer takes place in Cu_2O from oxygen to copper.[118] The peak ***1*** at 720 nm in case of $(Cu_2O)_3$ is found to be highest with full width at half maxima (FWHM) of 31.8 nm and that of $(Cu_2O)_2$ at 334 nm is lowest with FWHM of 13.6 nm among three sizes of the cluster (Fig. 5.8). Intensity of absorption is proportional to the product of square of OS and transition energy. The OS of peak ***1*** is lowest for $(Cu_2O)_2$ and highest for $(Cu_2O)_3$ while the OS of peak ***1*** of $(Cu_2O)_1$ with FWHM 7.28 nm is in between the two. Therefore intensity of absorption is lowest in case of $(Cu_2O)_2$ and highest for $(Cu_2O)_3$ (Fig. S5.1). Hence, it can be expected that variation of absorption intensity basically depends on nature of electronic transition. The calculated values of E_{exc} of Cu_2O quantum dots in table 5.2 shows the similar trend of quantum size effect as reported in reference [85] and thus validate the TDDFT results.

5.3.4.2 Effect of symmetry

In case of DDSCAT computation we have considered the effect of shape and associated symmetry of nanoparticles on the optical properties. During variation of symmetry the energy gap shift (ΔE) is predominantly regulated by ΔE^{kubo} and $\Delta E^{surface}$. To further verify how the interplay between ΔE^{kubo} and $\Delta E^{surface}$ play a crucial role in tuning optical features, TDDFT is performed by varying the symmetry of $(Cu_2O)_3$ to C_s, C_{2v} and C_{3v}. Elevation of symmetry causes change in structural parameters due to variation in coordination numbers. The Cu_{CSA} Cu_{CSA} bond length is shorter in C_{2v} compared to the C_{3v} geometry. Similarly the Cu_{CSA} $O_{CUS}{}^2$ bond length decends from C_{2v} to C_s. Consequently the relevant bond angles increases in higher symmetry, while the Cu_{CSA} O_{CUS} bond length remains approximately same in all the cases. The blue shift of E_{exc} of higher symmetry appears due to increase in $\Delta E_{occ-vir}$. For ease of analysis two types of peaks are chosen. Peak ***1*** corresponds to electronic transition of lowest excitation energy. The peaks are labelled as ***1_C_s***, ***1_C_2v*** and ***1_C_3v*** of their respective symmetries (Fig. 5.10a). The blue shift of peak ***1*** is attributed to ascending trend of $\Delta E_{occ\text{-}vir}$ with increase of symmetry from C_s to C_{3v}. (Fig. 5.10a and Table 5.3)

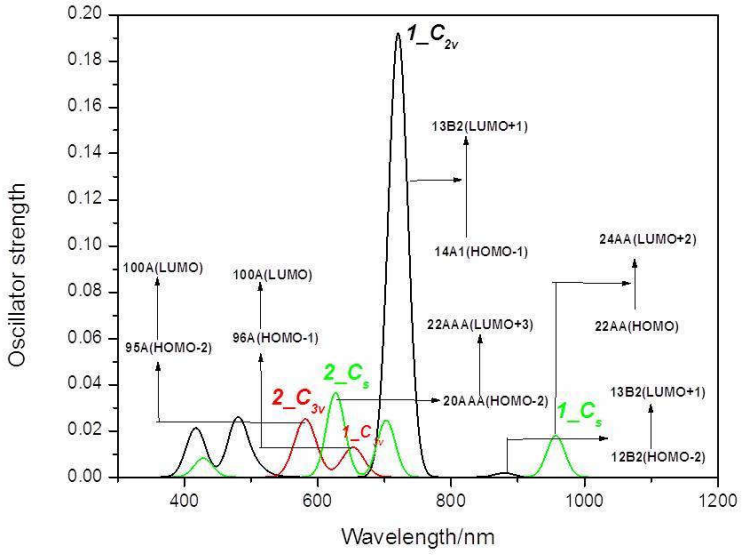

(a)

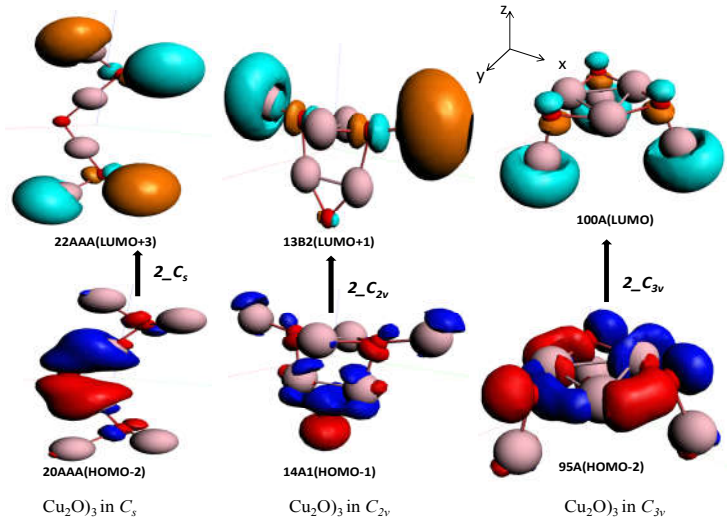

(b)

Figure 5.10 (a) TDDFT valence excitation spectra (oscillator strength vs excitation energy) of $(Cu_2O)_3$ clusters having different symmetries C_{2v} (red) and D_{3h} (black). The transitions with lowest excitation energy are reported as 1_C_s , 1_C_{2v} , 1_C_{3v} . The most intense discrete transitions are labelled as 2_C_s, 2_C_{2v} and 2_C_{3v} for respective symmetries. The MOs involved in corresponding transitions are also displayed. **(b).** The representation of MOs participating in the electronic transitions to form the most intense peaks labelled as 2_C_s, 2_C_{2v} , 2_C_{3v} for respective symmetries of $(Cu_2O)_3$ cluster. x, y and z are the reference axis of the MOs.

With increase of symmetry degeneracy of energy levels increase. On the contrary reducing the symmetry split the degenerate levels to multiple states, which is attributed to the highest $\Delta E_{\text{occ-vir}}$ value of C_{3v} and lowest of C_s. The other type of peaks labelled as **2** are chosen on the basis of electronic transition with highest oscillator strength. The peaks are labelled as ***2_C_s***, ***2_C_2v*** and ***2_C_3v*** according to the symmetry with ascending order (Fig. 5.10a). The peak ***2*** for C_{2v} symmetry (designated as ***2***_C_{2v}) is found to be most intense than the other peaks (designated as ***2_C_s*** and ***2***_C_{3v}). The proper reason behind the variation of OS can be explored by analysis of PDOS data and MO diagram (Table S2, Fig. 10b). The peak ***2***_C_{2v} is generated due to the transition from 14A1 to 13B2 (*vide supra*) whereas, peak ***2***_C_s and ***2***_C_{3v} are associated with transition from MO 20AAA to MO 22AAA and MO 95A to MO 100A. The transition from 14A1 to 13B2 in ***2_C_2v*** is purely LMCT type; whereas transition of 20AAA to 22AAA and 95A to 100A contains approximately equal *d* AOs contribution in ***2_C_s*** and ***2_C_3v*** respectively(Table S5.3 in ES5.I). Therefore oscillator strength varies linearly with extent of LMCT type transition. A remarkable agreement of the calculated values of E_{exc} of two different symmetries having approximately similar size (nanocubes and nanosphere) with reported results [119-120] confirms the reliability of TDDFT computation (Table 5.3)

Table 5.3 TDDFT data of discrete electronic excitations of Cu_2O clusters of same sizes in different symmetries. (a) is from reference (119)

Clusters	**Symmetry**	**Peaks**	**Occupied orbital**	**Virtual Orbital**	**$\Delta E_{occ-vir}$ (eV)**	**Oscillator strength**	**Excitation Energy (eV)**	**Reported excitation energy (eV)**
$(Cu_2O_3$	C_s	1	22AA(HOMO)	24AA(LUMO+2)	1.173	0.015	1.296	
		2	20AAA(HOMO-2)	22AAA(LUMO+3)	1.876	0.0302	1.98	
$(Cu_2O)_3$	C_{2v}	1	12B2(HOMO-2)	13B2(LUMO+1)	1.337	.0018	1.409	2.36[a] (420 nm)
		2	14A1(HOMO-1)	13B2(LUMO+1)	1.313	0.1923	1.72	2.407[a]
$(Cu_2O)_3$	C_{3v}	1	96A(HOMO-1)	100A(LUMO)	1.804	0.0064	1.898	2.25[b]
		2	95A(HOMO-2)	100A(LUMO)	2.017	0.0126	2.13	2.38[b]

5.3.5 Interpreting optical absorption spectra of Cu_2O NPs with TDDFT data

The analysis of electronic excitation of molecular clusters of $(Cu_2O)_n$ clearly reveals that the variation in absorption spectra of NPs with different size and shape depends on two factors. The shifting of spectra (blue or red) takes place due to the variation of gaps between energy levels (ΔE). The measure of ΔE in case of NPs is ΔE^{kubo} and in molecular cluster is $\Delta E_{occ-vir}$. The blue shift of spectra occurs when ΔE increases with decrease of size of nanoclusters. The second factor is the surface structure effect, which is dictated by the enhancement of $\Delta E^{surface}$ with increase of *S/V* ratio. This $\Delta E^{surface}$ contributes to the total energy gap (ΔE) and enhances the band gap value as well as absorption in NPs. The reason behind the increment of absorption can be rationalized by TDDFT results. The OS of excitation spectra predominantly depends on the nature of electronic transition among MOs. As it is suggested from earlier discussion, the nature of electronic transition depends on the structure of surface atoms. Two types of electronic transition takes place on Cu_2O surface, LMCT and MMCT. Reduction in coordination number of O at the surface increases the *p*-orbital-density at the valence band compared to conduction band. Thus, the valence to unoccupied orbital transition is dominated by ligand to metal transition when the surface is oxygen terminated. On the other hand the valence band will be dominated by *d* or *s* orbital of Cu if the surface is Cu terminated. This is clearly observed in the larger clusters calculation of $[Cu_{28}O_{15}]^{6+}$ and $[Cu_{44}O_{15}]^{6+}$ [Figure 11 5.(a) and (b)].

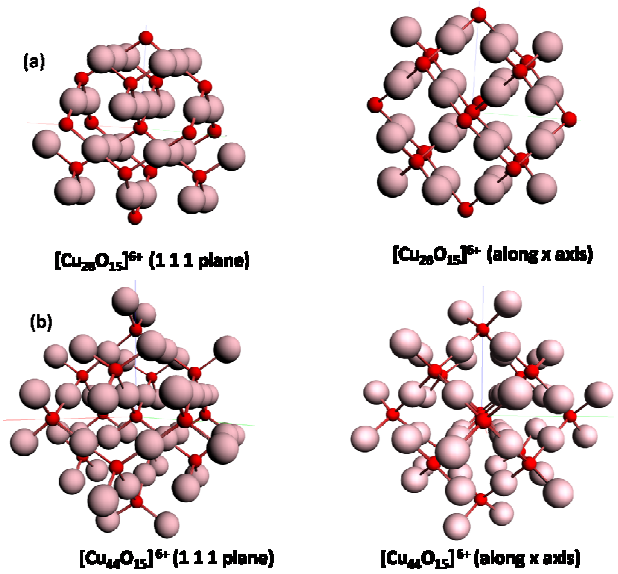

Figure 5.11 Molecular clusters of (a) $[Cu_{28}O_{15}]^{6+}$ and (b) $[Cu_{44}O_{30}]^{6+}$ in T_d symmetry.

Table 5.4 TDDFT data of discrete electronic excitations of larger Cu_2O clusters of different sizes in same symmetry.

	Symmetry	Peaks	Occupied orbital	Virtual Orbital	$\Delta E_{occ\text{-}vir}$ (eV)	Oscillator strength	Excitation Energy (eV)
$[Cu_{28}O_{15}]^{6+}$	T_d	1	71T2	38A1	2.157	.00024	2.2
		2	71T2	73T2	2.405	.00011	2.4
$[Cu_{44}O_{15}]^{6+}$	T_d	1	19A1	43T2	1.198	0.116	1.514
		2	19A1	44T2	1.567	.0268	1.786

The peaks are blue shifted with decrease of size (Figure 12(a) and (b)). This blue shift occurs due to increase of $\Delta E_{\text{occ-vir}}$ (Table 5.4). This result shows a similar trend and similar kind of electronic excitation (Table S5.5 in S5.I) behavior as the smaller clusters which is easily observable from Figure 5.12 **(a)** and 5.12 **(b)**. In both of the larger clusters the AOs of core part do not take part in the excitation, which is in accordance with the results obtained for smaller clusters (Figure S5.2).

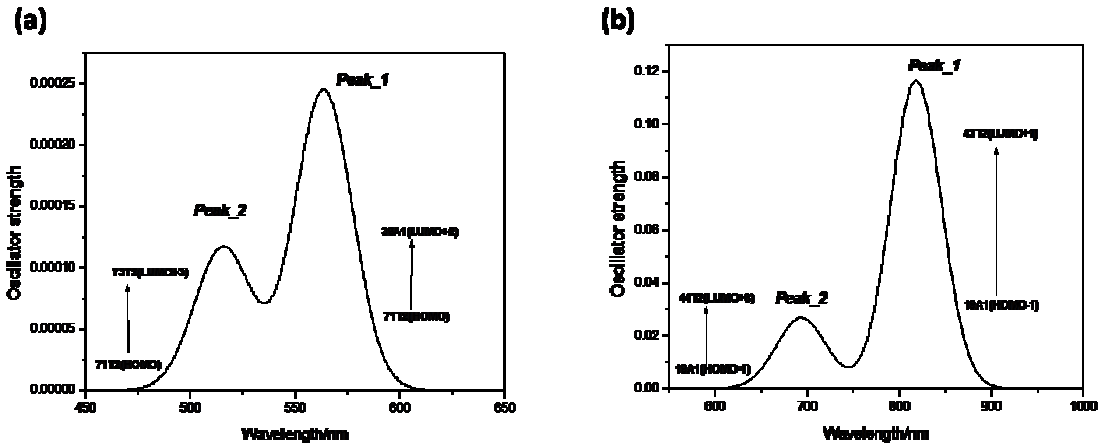

Figure 5. 12 TDDFT valence excitation spectra (oscillator strength vs excitation energy) of (a) $[Cu_{28}O_{15}]^{6+}$ and (b) $[Cu_{44}O_{30}]^{6+}$ in T_d symmetry. The most intense discrete transitions are labelled as *Peak_1*.

Enhancement of LMCT with lowering of cluster size can be attributed to the exposition of the O atoms to surface and thereby diminish their coordination environment. This is also observable from the simulated absorption spectra (Figs. 5.1a, 2a and 3a). Therefore, it can be concluded that the intensity of the peaks depend on the surface structure of nanoclusters. The peak intensity is influenced by LMCT if the surface is O-terminated and that of MMCT when the surface is Cu-terminated. Therefore, two types of peaks will arise, one of which is due to LMCT (O_{CUS}^{2} to Cu_{CUS}) and another is due to MMCT (Cu_{CSA} to Cu_{CUS}). The peaks due to LMCT are found to appear in the lower energy region, while the higher energy region is dominated by peaks of MMCT type. Bruneval *et al.* who have explored from DOS and energy distribution

curve (EDC) analysis that optical absorption spectra of Cu_2O arises from two distinct energy levels; one between -8 to -5 eV which is typically O 2*p* level and the other within -5 eV to Fermi level recognized as the Cu *d* level.[121] Therefore, the two distinct absorption peaks appearing in DDSCAT results is justifiable on the basis of the above observation.

5.4 Conclusion

The present work unravels the effect of surface structure reconstruction and variation in band gap upon their surface plasmon resonance and associated electronic transition of Cu_2O nanoparticles. The SPR peaks are found to be blue shifted with decrease in the size of the nanoparticles irrespective of the shapes, which is attributed to the increase of Kubo gap. This blue shift of SPR peak is also correlated with surface effect shift due to surface reconstruction during NP formation. As the shape of NP changes the related symmetry and *S/V* ratio also changes. Lowering of symmetry leads to splitting of degenerate energy levels. This is the reason behind the systematic change in optical response in between nanosphere and nanocube following the symmetry trend. The anomalous nature of optical response in case of cylinder can be explained from the enhancement of the band gap due to the inclusion of significant contribution of *S/V* ratio. The band gap varies linearly with *S/V* ratio as is apparent from Table 1. As a consequence the cylinder symmetry of Cu_2O NPs are following completely different trend. Irrespective of diameter, the surface plasmon wavelength maximum (λ_{max}) of the cylinder is completely blue shifted compared to sphere and cube. This is due to the largest band gap of the cylinders among the three shapes of same volume.

TDDFT computation is also performed to explore the phenomena of tuning optical response through surface structure reconstruction. The effect of size is traced by increasing the size of $(Cu_2O)_n$ with n =1, 2 and 3, keeping the C_{2v} symmetry intact. On the other hand, the effect of symmetry on absorption is studied for a specific cluster $(Cu_2O)_3$ varying its symmetry from C_{2v} to D_{3h}. The energy gap between occupied and virtual MOs ($\Delta E_{occ\text{-}vir}$), increases with decrease of cluster size from $(Cu_2O)_3$ to $(Cu_2O)_1$. Increase of symmetry leads to the blue shift of peaks, which is realized due to a increase in $\Delta E_{occ\text{-}vir}$. The reconstruction of surface induces the variation in structural parameters due to change in coordination number of the surface atoms. The nature of electronic transition depends on the coordination number of surface atoms. On this

account, two types of absorption occur on the surface of Cu_2O NPs. As the coordination number of O atom decrease the absorption becomes LMCT type and with decrease of coordination number of Cu atoms the absorption becomes MMCT type. A similar result of the increase in the size of NP is also tested with clusters of larger and more realistic sizes. The results invariably shows the same trend as is observed for smaller clusters. The blue shift in peaks with decrease in size is attributed to the increase of $\Delta E_{\text{occ-vir}}$. Therefore we can conclude that with change of size and symmetry the variation of two major factors play an important role to tune the absorption as well as surface plasmon resonance of Cu_2O nanoclusters.

In the present work, it has been systematically shown that the optical property, i.e., SPR, absorption, and scattering can be tuned by manipulating size and symmetry of Cu_2O nanostructures. Hence, these observations find sophisticated applications in the fields of biosensors, solar cells, photodiodes, photo catalysts etc. [13-17] With the increment of size of Cu_2O nanospheres the value of scattering coefficients become larger than the gold sphere, which is already employed for the selective imaging of cancer cells.[122,123] The Cu_2O nanospheres of D = 140 nm, 160 nm, 180 nm, 220 nm, and 240 nm have ε_{sca} greater than that of gold NPs. So these size ranges for Cu_2O nanospheres can be used as cell imaging and detection of proteins as reported earlier.[73] Therefore, this work can also guide the selection of appropriate size and shape of nanoclusters with desired band-gap for some specific application.